Available online at www.eccomasproceedia.org
Eccomas Proceedia COMPDYN (2023) 2640-2655

ECCOMAS
Proceedia

COMPDYN 2023
9th ECCOMAS Thematic Conference on
Computational Methods in Structural Dynamics and Earthquake Engineering
M. Papadrakakis, M. Fragiadakis (eds.)
Athens, Greece, 12-14 June 2023

SENSITIVITY ANALYSIS OF DRY-JOINT STONE MASONRY WALLS USING DISCRETE ELEMENT METHOD

Ciro Canditone[1], **Fulvio Parisi**[1]

[1] Department of Structures for Engineering and Architecture
University of Naples Federico II, Via Claudio 21, 80125 Naples, Italy
e-mail: {ciro.canditone, fulvio.parisi}@unina.it

Abstract

Masonry has historically been amongst the most widely used building materials, hence being observed in a large percentage of the historical built heritage in many countries. Many historical masonry buildings include structures made of dry-joint stone masonry (DSM) walls, due to either original building techniques or significant mortar loss under various degradation sources. In this latter case, partial or total mortar loss under combined chemical, mechanical and physical degradation may indeed lead to a material behaviour akin to that of dry-joint masonry. Research on structural behaviour of DSM buildings, including experimental and/or theoretical studies, is therefore required to assess and mitigate disaster risk in several countries.

In this study, the discontinuous nature of dry-joint masonry and its complex nonlinear response is numerically modelled according to the discrete element method (DEM). In such a discontinuum-based micro-modelling approach, masonry is discretized into an assembly of distinct bodies, either rigid or deformable, which are locally connected by pairs of normal and tangential springs simulating the interface behaviour. Large-displacement dynamic analysis accounting for separation and impact between bodies is thus carried out, allowing the simulation of fracture and collapse processes. In case of dry-joint stone masonry, a numerical model is validated against experimental data and a discussion over the advantages and limitations of the adopted modelling approach is provided. The model is then used to run a parametric analysis on DSM elements, in the form of either individual structural components or assemblies. Due to their relevance in the overall structural behaviour of masonry buildings under both gravity and horizontal loads, DSM piers are investigated, in order to assess the sensitivity of their mechanical behaviour to aspect ratios, load and boundary conditions.

Keywords: stone masonry; discrete element modelling; experimental validation; sensitivity analysis; force-displacement behaviour; crack pattern.

ISSN:2623-3347 © 2023 The Authors. Published by Eccomas Proceedia.
Peer-review under responsibility of the organizing committee of COMPDYN 2023.
doi: 10.7712/120123.10590.20983

1 INTRODUCTION

Masonry is amongst the most common and traditional building techniques. As such, its use characterizes some of the most important cultural and historical monuments, as well as a large part of the building stock of both developed and underdeveloped countries. It is, however, a material known to exhibit a remarkable vulnerability, especially when subjected to seismic loading.

Masonry can be seen as a composite, discontinuous material made up of an assembly of (i) units (either regular or irregular, stone, clay or earthen made), (ii) joints (either dry or mortared), and (iii) contact interfaces. The case of dry-joint stone masonry (DSM) is of particular interest, due to this building technique having been widely used in the archaeological and historical heritage of many countries.

Moreover, a condition akin to that of DSM can be found in many historical and archaeological stoneworks which, originally built with mortared joints, have undergone phenomena of mortar degradation and loss. In those cases, the combination of physical, mechanical, and chemical actions may indeed lead to mortar strength loss, mortar erosion and weakening of the unit-to-mortar bond, leading in turn to a behaviour resembling that of dry-joint masonry.

Research into the area of dry-joint masonry is, thus, essential to provide a better understanding of its behaviour under external loads and to support decision-making in favour of its repair and/or strengthening. In this regard, experimental testing – either in-situ or in laboratory conditions – can indeed provide valuable information, but full-scale tests are known to be time consuming, expensive, and difficult to conduct. Indeed, existing literature over DSM experimental testing is quite limited, more so in the case of irregular dry joint masonry.

Experimental testing mainly focused on small scale tests, and especially on interface mechanical properties' characterization [1–3]. Such studies highlighted DSM's remarkably nonlinear behaviour, characterized by complex phenomena such as joint closure under compressive loads and geometric imperfections in the joint surface influencing joint strength. Overall, nonlinear behaviour at joint level under combined normal and shear loads is well described in studies such as [4–6].

The scale of small-scale masonry specimens was tackled, too. Remarkable nonlinearity was in fact confirmed at wallette scale by [7] and [8], which studied the behaviour of DSM wallettes subjected to precompression load and, respectively, in-plane and out-of-plane horizontal loads. However, research into large scale specimens is still lacking, translating into knowledge gap over the behaviour of structural components such as DSM piers.

In this regard, computational tools might play a fundamental role. A numerical model, validated onto numerical results, might indeed be used to expand the scope and range of complex problems and scenarios otherwise difficult to investigate, leading to that upscale from masonry panels to full-size load-bearing components needed to fill the knowledge gap.

This paper, thus, aims at improving the knowledge of the in-plane behaviour of dry joint masonry piers by means of numerical tools. A simplified rigid-block and zero-thickness interface micro-model, implemented in DEM (Discrete Element Method) software package 3DEC, was first validated against experimental data available in [7] before being applied to run parametric analyses aimed at a characterization of the behaviour of four DSM piers taken as case studies. Novelty of the study, thus, lies in providing further insight over the structural behaviour of DSM structural components for which experimental tests might be prohibitive.

The following parameters were considered: two aspect ratios (H/L=2, H/L=1), two boundary conditions (cantilevered and doubly-fixed piers) and three different precompression levels, defined in terms of axial load divided by ultimate axial load (N_s/N_u). This produced 12 combinations of those parameters, hence resulting in the same number of pier configurations.

Results were then collected in terms of force–displacement curves, crack patterns and failure modes, to discuss the numerically evaluated behaviour of DSM piers both in qualitative and quantitative terms, attempting to provide insight on their nonlinear behaviour under in-plane lateral loading.

2 METHODOLOGY

2.1 Numerical modelling strategies

Several strategies are available for numerical modelling of masonry. According to [9], a distinction can be made between the following computational strategies: (a) macro-modelling strategies, in which masonry constituents, that is, units, joints and contact interfaces, are smeared into one equivalent continuum with homogenized properties; (b) advanced micro-modelling strategies, in which units, joints and contact interfaces are modelled individually; and (c), simplified micro-modelling strategies, in which units are represented as a discontinuous series of discrete bodies interacting through zero-thickness interfaces, which capture joint behaviour. The latter approach was here selected, based on its overall good trade-off between accuracy and computational effort, and was implemented within a Discrete Element Method (DEM) framework, based on its well-proven ability to model continuum as well as discontinuum problems involving large displacements and/or material fracture and separation.

The formulation, initially developed by [10, 11] for the study of jointed rocks, was in fact subsequently employed with success to study other discontinuous media, such as masonry. Studies over the suitability of DEM to replicate the experimental behaviour masonry can be found, amongst others, in [12,13,14], while [15] focused specifically on simulating the behaviour of dry joint masonry under in-plane and out-of-plane actions.

For a detailed description of the method, as well as the available modelling strategies which can be implemented in DEM to simulate masonry – which is beyond the scope of this paper – the reader is redirected, amongst others, to [10-16]. It is noted that, in DEM-based software packages such as 3DEC, masonry is usually modelled as either (a) an assembly of rigid blocks, with system deformability lumped into the nonlinear zero thickness interfaces, or (b) an assembly of linear elastic, isotropic deformable bodies and nonlinear interfaces, in which case system deformability needs to be carefully distributed onto both constituents.

The first approach saves considerable computational time, at the expense of the model's ability to capture phenomena related to unit deformability or inelastic behaviour, such as compressive failure due to the crushing of the blocks, or tensile failure leading to unit splitting. Despite this, however, the method seems to be quite suitable to model those cases, such as low-bond strength mortar joints or dry joints, in which unit deformability plays little role and failure is governed by mechanisms [17].

Thus, as will be seen in the next sections, a rigid block and zero-thickness nonlinear interface-based model was chosen and used to replicate experimental data before being validated and extended to larger scale problems.

2.2 Model validation against experimental data

To assess the reliability of 3DEC and of the selected modelling approach for in-plane quasi-static analysis of DSM, data from experimental tests over DSM wallettes [7] was compared with numerical analyses. Within the selected study, seven single-leaf, DSM wallettes with size equal to $1.0 \times 1.0 \times 0.2$ m^3 (height by length by thickness) were tested under combined precompression and horizontal loads. Four different precompression loads were investigated (30 kN, 100 kN, 200 kN, 250 kN) and results were collected in terms of damage pattern and load-

displacement curves. Through this experimental campaign, Lourenço et al. [7] got the following findings:

a) a relationship between applied compression load and Young's modulus, E, of the specimens;

b) remarkably nonlinear behaviour under horizontal loads, with relevant excursion in the post-elastic phase and very significant drift levels (always higher than 2.5%);

c) failure mode linked with applied compression load, with lower compression loads leading to diagonal joint sliding and rigid body rocking of the upper diagonal around a hinge, and higher compression loads correlated with diagonal cracking coupled with unit splitting or crushing at the compressed toe.

In this regard, however, it should be noted that maximum initial compressive stress imposed, equal to 1.25 MPa, is far lower than the experimentally evaluated compressive strength of the dry-stacked masonry here considered [18] (mean value equal to 57.13 MPa and coefficient of variation CoV = 22%), pointing to compressive stresses increasing due to second order effects under increasing horizontal displacements.

Furthermore, the authors proposed equations to evaluated normal and tangential joint stiffness, K_n and K_s, there implemented in a DFEM (Discrete-Finite Element Method) numerical model, and here used in a DEM framework. These equations correlate joint stiffness with unit Young's modulus, E_b, unit height, h_b, Poisson's ratio, v, and Young's modulus of masonry, E_m.

The mechanical properties implemented within the numerical models are summarised in Table 1, where the above-mentioned experimentally variations in stiffness with axial load are outlined.

Model	ρ [kg/mc]	ϕ [°]	K_n [MPa/mm]	K_s [MPa/mm]
SW-30	2200	30	5.87	2.45
SW-100			8.08	3.37
SW-200			11.34	4.73
SW-250			13.03	5.43

Table 1 - Mechanical properties used in 3DEC for model validation

Precompression load was modelled here by altering the self-weight of a rigid block applied on top of the wallette to redistribute loads, simulating the reinforced concrete beam used in the experiments for the same purpose. Lateral load was modelled as displacement-controlled, by assigning this top block a constant horizontal velocity which was selected equal to v=1 mm/s after sensitivity analyses confirmed no undesired inertial effects developed. Further parametric analyses led adopting a number of contact points per each interface n=5, as it yielded a good compromise between computational time and solution stability. The numerical model employed can be found in Figure 1.

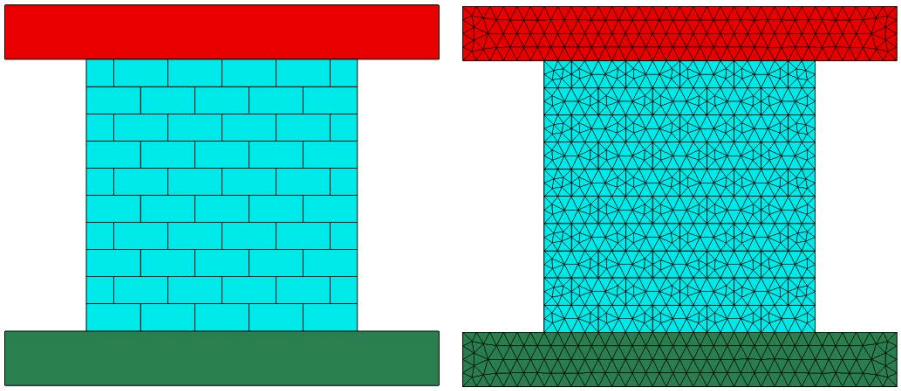

Figure 1 - Plain and meshed views of DE model for simulation of experimental results

A comparison between simulated and observed crack patterns is shown in Figure 2, whereas load–displacement curves are shown in Figure 3.

Comparing the crack patterns from numerical and experimental data, good agreement is found, with the main experimental failure modes – opening of a diagonal crack, right to left – being adequately represented. It should be worth noting that, as all nonlinearities were here lumped into the interfaces, value of friction angle φ was found significantly influence maximum shear capacity and crack pattern, with values of φ lower than 30° leading to horizontal slip of the top joints rather than the observed diagonal slip failures.

Owing to the modelling assumption of rigid blocks, the numerical model could not, however, capture localized phenomena of cracking and crushing of stone blocks, which were witnessed experimentally for higher values of compression load.

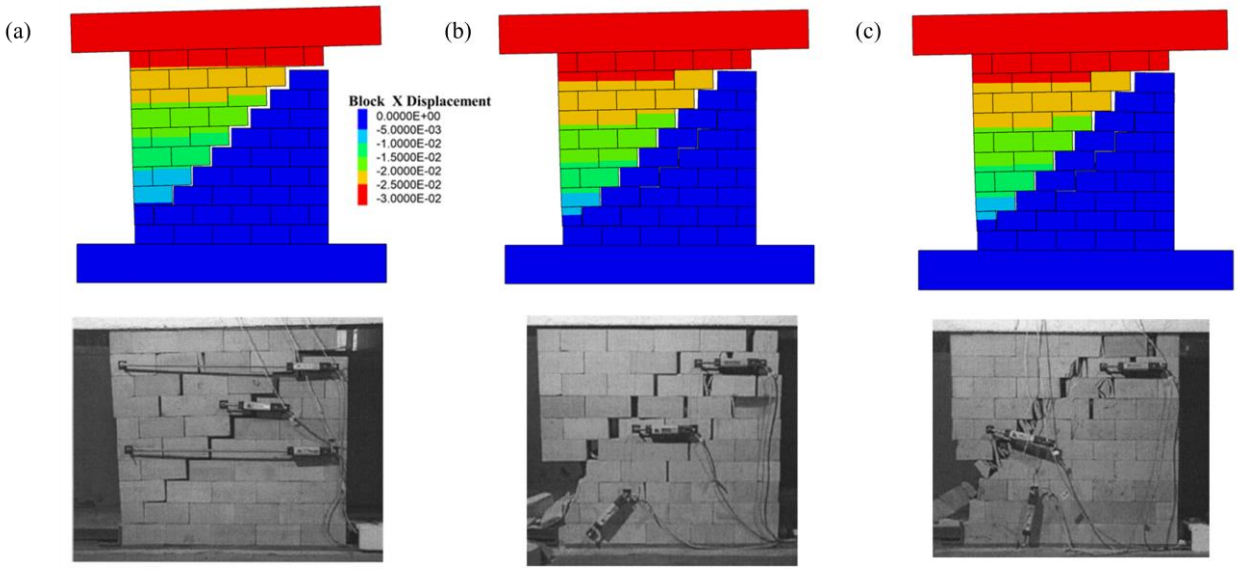

Figure 2 – Comparison between numerical and experimental crack patterns for: (a) SW30; (b) SW100; (c) SW200; (pictures adapted from [7])

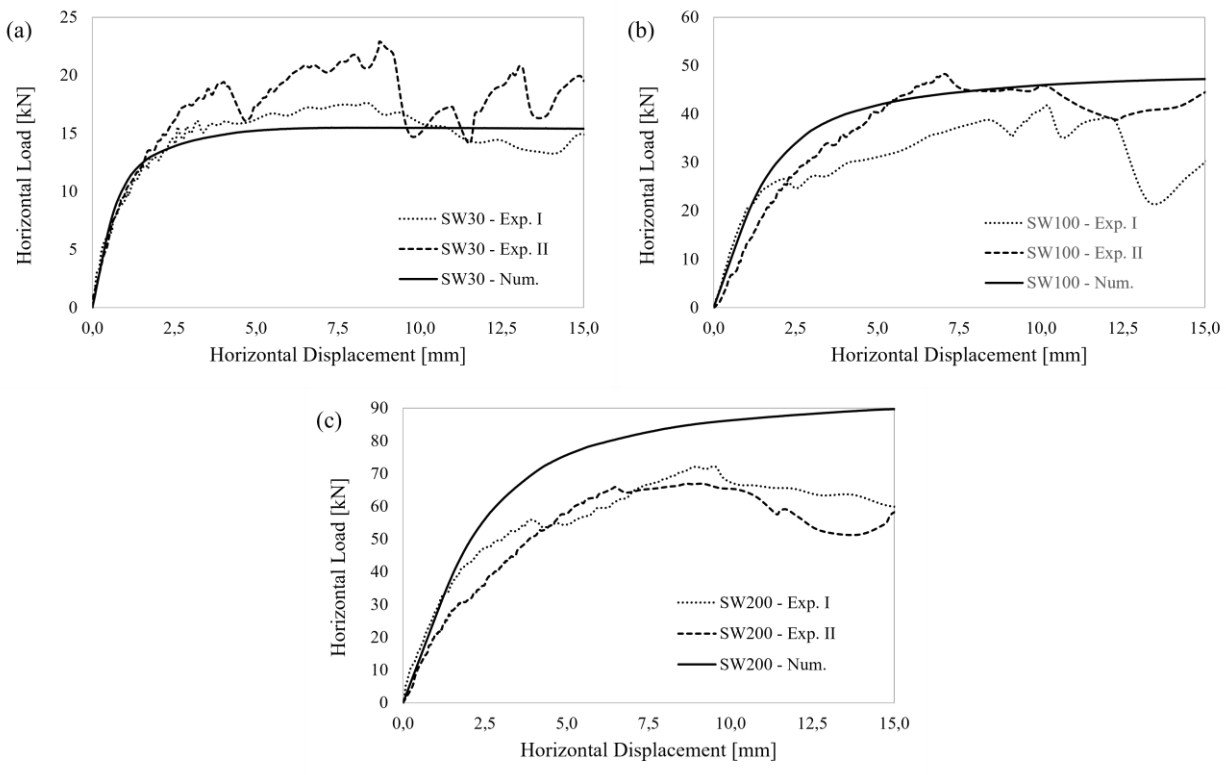

Figure 3 - Numerical versus experimental curves corresponding to different precompression levels: (a) 30 kN, (b) 100 kN, (c) 200 kN

In terms of load-displacement curves, the numerical models captured well the initial stiffness of SW30, SW100 and SW200 wallettes, as well as their displacement capacity. In terms of peak strength, a good match is found for SW30 and SW100 specimens – numerical values of maximum shear being, respectively, 30.1% lower, and 4.9% higher than their experimental counterparts – while an overestimate is found for SW200 wallette, peak numerical shear 29.9% higher than the experimental one.

Wallette	Lourenço et al. (2005)		Bui et al. (2017)	Liu and Crewe (2019)	Present study (2022)
	Experimental	FEM	DEM - RB	DEM - RB	DEM - RB
SW30	22.4	17.0	15.7	15.4	15.5
SW100	45.0	47.5	48.5	49.0	47.3
SW200	70.3	81.4	93.0	90.0	91.3

Table 2 - Comparison between numerical results and data available in the literature

However, as can be seen in Table 2, numerical results of the present study are comparable with those found in [7, 13, 17]. The three referenced DEM studies employing rigid blocks achieved very similar error margins for all three case studies, with the D-FEM model in [7] yielding slightly better, yet still overestimate, results than DEM for high compression values.

Thus, despite this inability to capture local failure due to crushing or splitting – which should be taken into account by using the approach cautiously and complementing it with other numerical or analytical tools – the validation case here presented should prove the suitability of rigid block-based DE to capture the experimental results with acceptable degree of accuracy, thus supporting further numerical studies on DSM piers.

3 DEM ANALYSIS OF DSM PIERS

3.1 Geometry, loading and material properties of the DSM piers

A total of 12 different DE models were here considered, by combining two aspect ratio parameters (α_1=*H/L*=2 and α_2=*H/L*=1), two boundary conditions (cantilevered pier, C, and doubly-fixed pier, DF), and three different axial load ratios between axial load N_s and ultimate load N_u (i.e., N_1=5%, N_2=15% and N_3=30%).

Variability of such parameters was deemed representative of load-bearing piers inserted in larger DSM assemblies, in terms of geometry, axial loading and degree of interaction with adjacent spandrels, thus enabling nonlinear analysis of DSM structures under combined in-plane vertical and horizontal loads.

The combination of the above-mentioned conditions and parameters produced 12 pier configurations, the geometric and loading features of which are collected in Table 3. Those configurations were named according to the following rule: B-α_n-N_n, with B being the boundary condition (C, cantilevered, or DF, doubly-fixed), α representing aspect ratio, and N_n representing the ratio of N_s to N_u. The DE models employed are instead shown in Figure 4.

Model	*T* [m]	*H* [m]	*L* [m]	*Ns* [kN]	N_s/N_u
C1 N1 / DF1 N1	0.20	2.00	1.00	571.25	5%
C1 N2 / DF1 N2				1713.75	15%
C1 N3 / DF1 N3				3427.50	30%
C2 N1 / DF2 N1			2.00	1142.50	5%
C2 N2 / DF2 N2				3427.50	15%
C2 N3 / DF2 N3				6855.00	30%

Table 3 - Geometric and loading configurations under investigation

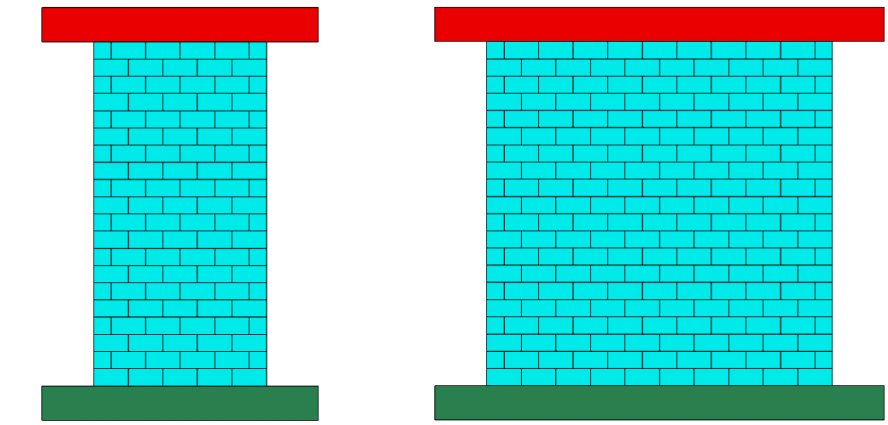

Figure 4 - DE models of DSM piers with aspect ratios α_1=2 and α_2=1

Concerning material properties (see Table 4), density ρ and friction angle φ were kept the same as those used to validate the model against experimental data in [7], as were also kept stone unit geometries (100x100x200 mm^3 and 200x100x200 mm^3). However, in the definition

of K_n and K_s stiffness values, a choice was made to consider E_m as a value independent from the axial load, opposed to what was done in Section 2.

The phenomena of joint closure witnessed in [7] which led to variations in stiffness under increasing compression load and which were accounted for by varying K_n, K_s for each wallette, should in fact progressively stabilize under increasing load and play little to no role at the levels of normal stresses here considered. Thus, a choice was made to assume the experimental value of E_m=2280 MPa (CoV 6.2%) given in [18] for the same kind of DSM.

ρ [kg/mc]	ϕ [°]	K_n [MPa/mm]	K_s [MPa/mm]
2200	30	16.36	6.82

Table 4 - Mechanical properties used in 3DEC for the modelling of DSM piers

Precompression loads were modelled through self-weight of the top beam, and a displacement-controlled horizontal load imposed by means of a horizontal velocity v=1 mm/s at top beam centroid. In-plane target displacement was taken as Δ_{max}=200 mm, that is, the whole length of a unit, while out-of-plane displacements were inhibited, to fully exploit in-plane capacity. Finally, normal stresses at block contacts were also monitored, to keep an eye on possible mechanisms of unit splitting and crushing not explicitly modelled.

3.2 Numerical results

Results from numerical analyses were collected in terms of crack pattern, load-displacement curves, evolution of applied normal load and normal stresses at block contacts. Ultimate conditions were assumed as a load drop ΔV=20%; regardless, numerical results up to convergence loss were plotted, too, with dotted lines. Whenever such ultimate condition was not met before Δ_{max}, anyway, ultimate shear V_u was taken as the last recorded value.

Load-displacement curves were then bilinearized to evaluate displacement ductility μ_Δ.

Overall, analysis results in terms of peak shear V_{max}, corresponding displacement Δ_{Vmax}, residual shear V_u, corresponding displacement Δ_u, displacement ductility μ_Δ and occurrence of normal stresses σ_c reaching peak compressive strength f_c are recollected in Table 5.

Model	N_s/N_u	V_{max} [kN]	V_u [kN]	Δ_{vmax} [mm]	Δ_u [mm]	$\mu(\Delta)$	$\sigma_c > 0{,}8f_c$
C1 N1	5%	108.7	87.0	56.6	169.0	10.7	FALSE
C1 N2	15%	257.6	206.1	88.6	190.5	5.0	TRUE
C1 N3	30%	385.7	319.6	122.9	200.0	3.1	TRUE
C2 N1	5%	490.1	392.1	60.7	111.6	7.4	TRUE
C2 N2	15%	1280.4	1107.4	97.0	186.6	5.0	TRUE
C2 N3	30%	2270.2	2141.1	153.0	200.0	3.0	TRUE
DF1 N1	5%	344.1	275.3	83.0	98.6	3.1	FALSE
DF1 N2	15%	681.9	546.2	112.0	148.5	3.8	FALSE
DF1 N3	30%	1107.7	886.1	139.1	193.8	4.8	TRUE
DF2 N1	5%	695.8	556.6	71.7	100.8	5.6	FALSE
DF2 N2	15%	1486.7	1189.4	65.7	121.6	5.2	TRUE
DF2 N3	30%	2595.7	2259.2	91.3	154.8	3.9	TRUE

Table 5 - Summary of numerical results

Load-displacement curves are instead provided in Figure 5. As can be seen, said curves are characterized by an initial linear elastic phase up to 55% (CoV = 14%) of maximum horizontal load, followed by nonlinear, approximately parabolic behaviour up to maximum peak shear. After peak strength is achieved, load gradually drops through softening phases which seem more stable in cantilevered (C) piers than in doubly-fixed (DF) piers. All considered configurations exhibit considerable displacement capacity, with minimum Δ_u equal to 98.6 mm and several piers reaching Δ_u in the 190-200 mm range.

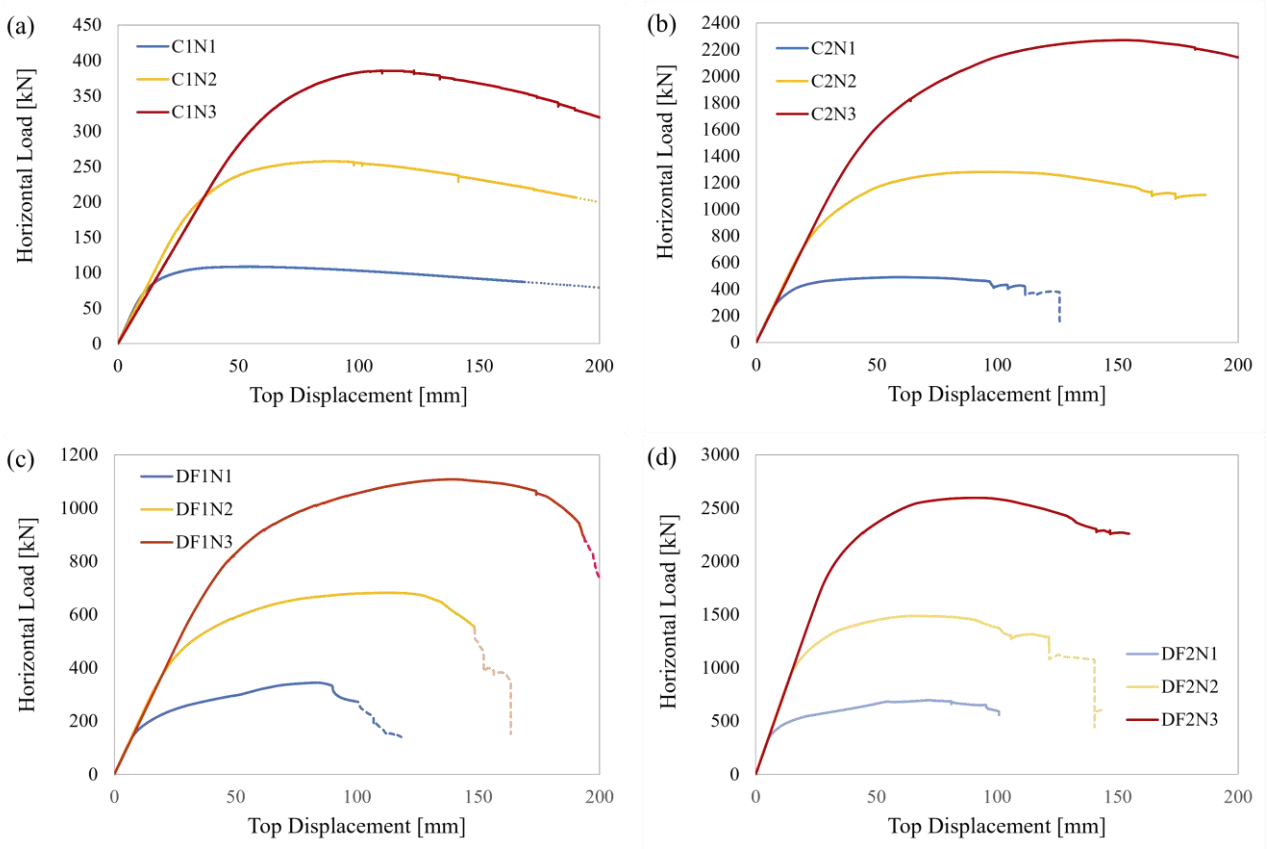

Figure 5 - Load-displacement curves of different piers under three precompression levels (N1, N2, N3): (a) C1, (b) C2, (c) DF1, (d) DF2

A generalized positive trend associating higher values of strength and larger ultimate displacements with increasing precompression levels is found. While the positive correlation between applied normal load and maximum horizontal stresses is expected in DSM and masonry in general, as it can be described as a material obeying to a Mohr-Coulomb criterion – by which maximum shear stresses are described as a linear function of applied normal stresses – the second is quite unexpected.

Experimental studies over the displacement capacity of URM, for which results a comprehensive review can be found in [20], found in fact ultimate displacement capacity to decrease with increasing precompression loads. It should be noted, however, that other factors, including failure mechanisms, material properties and geometry play a role in the deformation capacity, and should thus be considered.

Possible explanations for the positive trend here encountered will be thus provided in the next section, coupled with a discussion over the failure modes encountered.

3.3 Interpretation of failure modes

Typically, in-plane failure mechanisms of URM walls fall into one of the following categories: (a) sliding shear failures, (b) diagonal shear mode, (c) rocking and flexural failures, or (d) hybrid failures, when combined shear and flexural failures occur. Deformation capacity of URM walls under in-plane horizontal loads has been proven to depend mainly on failure mode. Indeed, the so-called diagonal shear failures, which occur as a result of tensile stresses exceeding tensile strength, are associated with smaller displacement capacity than phenomena of simple shear sliding or rocking [20]. These phenomena are in fact associated to very large displacement capacities, for which an upper threshold is given more by *P-Δ* effects and equilibrium loss rather than strength [21].

Thus, interpretation of numerically evaluated failure modes may provide considerable insight into these DSM piers' large displacement capacity and ductility.

Crack pattern of cantilevered (C) and doubly-fixed, shear-type (DF) piers is provided in Figures 6 and 7, respectively, together with a plot of the horizontal displacement along the height of the wall.

Analysis of the above-mentioned deformed shapes and crack patterns at ultimate displacement Δ_u, complemented with the analysis of normal stress distributions at block contact points, allowed the following phenomena to be identified: (a) shear sliding along one or more diagonals; (b) rocking; and (c) toe crushing. Such failure modes often interact with each other, producing a mixed failure mechanism. All considered, the following failure mechanisms at global, pier scale were identified:

a) sliding shear along one or more diagonals;
b) sliding shear along one diagonal, coupled with rocking behaviour;
c) sliding shear along one or more diagonals, coupled with toe crushing.

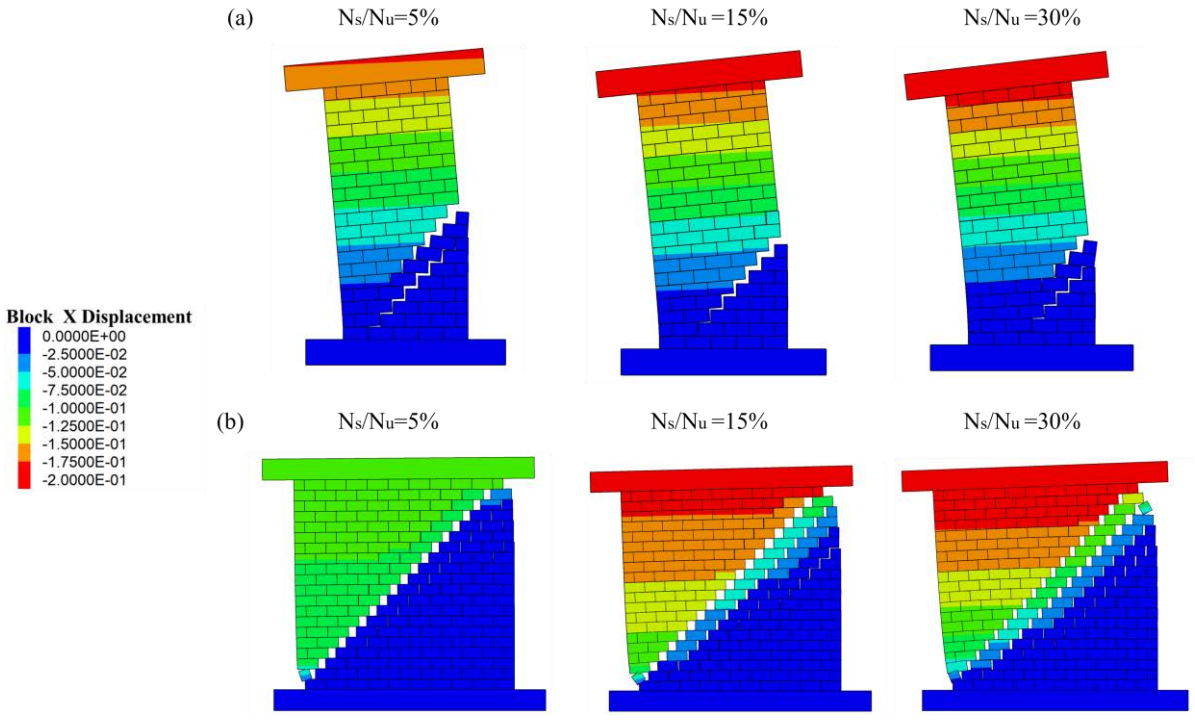

Figure 6 – Ultimate crack pattern and configuration of the following cantilevered piers: (a) slender (C1) and (b) squat (C2)

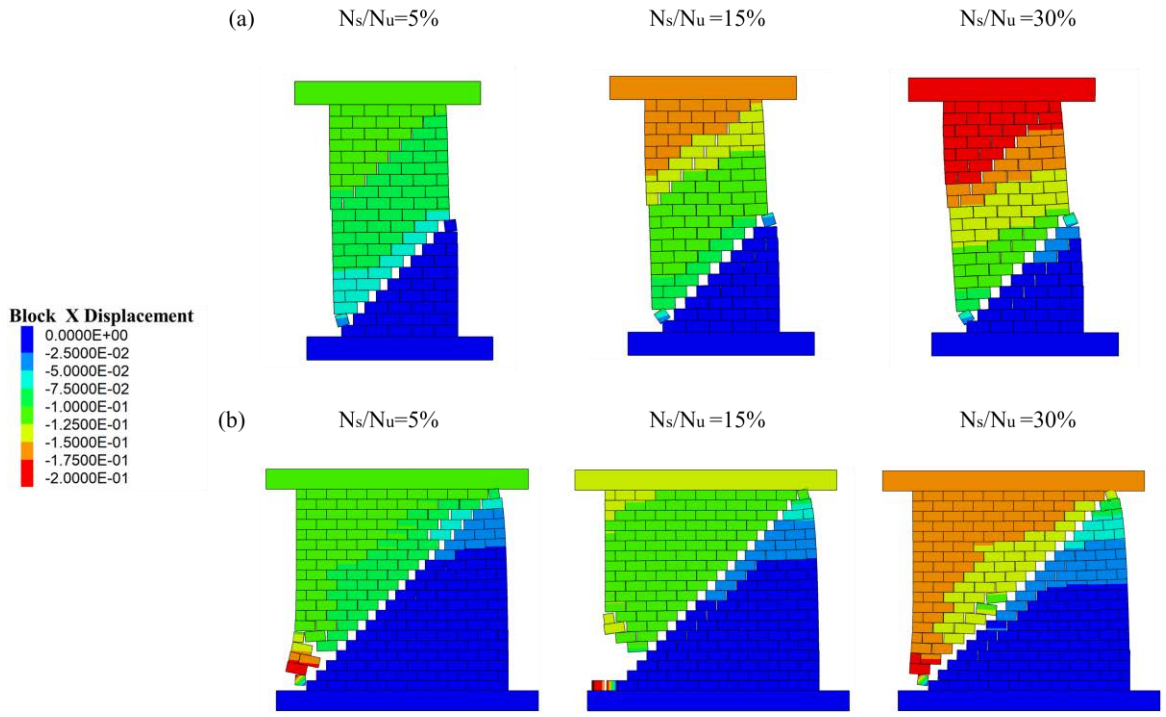

Figure 7 – Ultimate crack pattern and configuration of the following doubly-fixed piers: (a) slender (DF1) and (b) squat (DF2)

At local level, these mechanisms, coherently with the physical reality of DSM, occur as a result of either (a) joint failure in pure sliding (explicitly considered within the numerical model) or (b) unit failure under splitting or crushing (here considered monitoring normal stresses at interface level). Large displacement capacity is associated with joint sliding and rocking behaviour. Indeed, the larger displacement capacities numerically evaluated (C1N1, C1N2, C1N3, C2N2, C2N3, DF1N3, all exhibiting displacements greater than 150 mm) are associated with either the development of sliding failures along more than one diagonal, thus invoking the displacement capacity of many joints, or the development of joint sliding along one diagonal followed by rocking phenomena. Mechanisms of simple joint sliding followed by rigid body horizontal translations (DF1N1), or diagonal joint sliding coupled with toe disaggregation and equilibrium loss (DF2N1, DF2N2, DF2N3), produced far smaller ultimate displacements.

The comparatively large displacement capacities developed by the DSM piers, and the positive trend associated with larger precompression levels, can thus be explained as follows: larger N_s/N_u values are associated with either (a) more diagonal bands failing in sliding shear (mechanism characterized by large displacement capacity) or (b) rocking behaviour of slender, highly deformable configurations such as the cantilevered (C) piers. Whenever the axial load or boundary conditions did not allow the formation of multiple slip failures, or equilibrium loss occurred because of corner disaggregation, the displacement capacity did not attain large levels.

Finally, it should be noted that much of the existing knowledge on URM piers' displacement capacity, and its interaction with axial load, is based on mortared masonry. In [20], the referenced tests are limited to clay brick and bed joints with general purpose mortar; out of 71 specimens, 34% of them suffered diagonal shear failures, 31% flexural failure, and 29% mixed failures. Only 4% of specimens failed in sliding.

Thus, investigation over the large displacement capacity associated with joint sliding seems underrepresented in literature, particularly in case of DSM piers for which the phenomenon clearly plays a key role as one of the only two possible local failures.

Available experimental investigations over the in-plane behaviour of DSM seem to provide evidence in support of this large displacement capacity, with quite large drift values being achieved at various levels of normal stress [7]. Though, admittedly, the authors tested the specimens under low stress regime – no greater than 2% of the ultimate load – Δ_u values seemed unaffected by normal load variations and thus current experimental findings do not exclude a positive correlation.

Hence, a knowledge gap might subsist over the displacement capacity of DSM piers and its possible positive interaction with axial load. Further experimental testing might be needed to prove or disprove the numerical findings here gathered.

3.4 Influence of boundary conditions

The effects of the various parameters here investigated – aspect ratio α, boundary conditions B and applied precompression ratio N_s/N_u – were assessed by comparing normalized shear load V_{max}/N_u, ductility ratios – defined by means of bilinearization of the pushover curves – and failure patterns. Analyses results are aggregated in Figure 8.

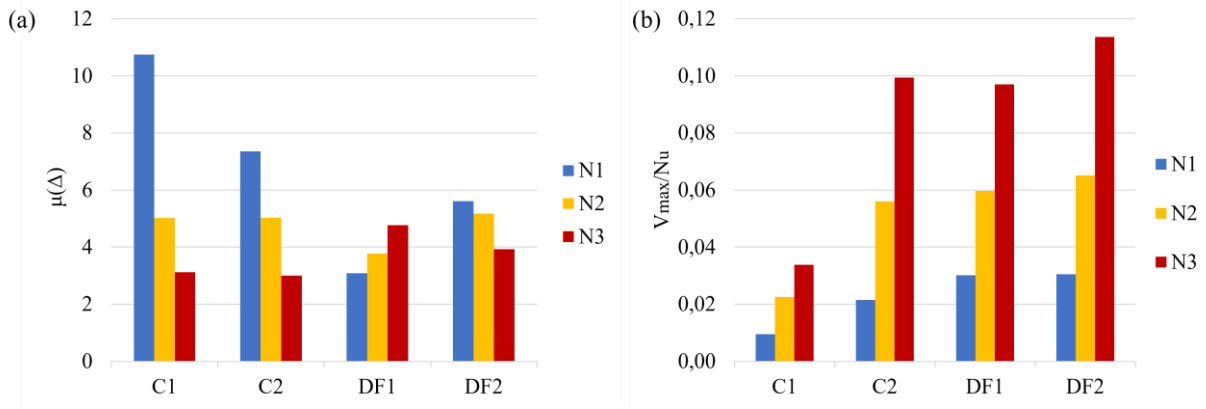

Figure 8 - Effects of boundary conditions and precompression ratio on (a) maximum dimensionless shear and (b) displacement ductility.

In terms of the effects of boundary conditions B on normalized shear load, it was found that, given the same aspect ratio α and N_s/N_u ratio, doubly-fixed, shear-type piers exhibited a better performance than corresponding piers in a cantilevered condition.

When considering slender piers (α_1=2), doubly-fixed piers displayed a normalized shear capacity 3.17, 2.65 and 2.87 times higher than the corresponding cantilevered piers for N_1, N_2 and N_3 compression ratios, respectively. This effect seems less remarkable for squat (α_2=1) piers, for which normalized shear is 1.42, 1.16 and 1.14 times higher than that of squat cantilevered piers at N_1, N_2, N_3 compression ratios.

When considering the interaction between boundary conditions and displacement ductility μ_Δ, instead, cantilevered piers were found to be considerably more ductile than corresponding doubly-fixed walls, coherently with available experimental knowledge [20], which proves specimens in doubly-fixed conditions to display lower drift values than those with cantilevered boundary conditions. Indeed, slender cantilevered piers reached a displacement ductility that was 3.49, 1.33 and 0.65 times higher than that shown by doubly-fixed piers for the same

precompression ratios. Similarly to what was observed for normalized shear, the effects seems less relevant for squat piers, for which C/DF ductility ratios range between 1.31 and 0.77.

When considering failure mechanisms, it would seem, as it would be reasonable to expect, that a key role is played by the interaction between boundary conditions B and aspect ratios α. Failure mechanism seems in fact heavily influenced by these two parameters, with slender cantilevered piers (C1) being subjected to combined shear and rocking, and all slender doubly-fixed piers (DF1) failing by means of the formation of two diagonal crack bands passing through the joints and relative rigid translation between these two bands. This is coherent with experimental data, as rocking and flexural failures are to be expected from slender structures with a high moment/shear ratio [20], which is particularly true for cantilevered piers.

Likewise, all squat shear-type piers (DF2) displayed the same failure mechanism, that is, formation of a single diagonal crack followed by toe crushing and corner disaggregation, while a more complex interaction between applied precompression load ratio N_s/N_u, boundary conditions B and aspect ratio α was found for squat cantilevered piers (C2).

3.5 Influence of precompression load

As done for boundary conditions, the effects of precompression ratios N is herein discussed in terms of normalized shear and ductility rations (see Fig. 8), as well as influence on crack pattern and failure mechanism.

Given the same boundary condition B and aspect ratio α, there seems to be a positive correlation between precompression ratio N and normalized shear load V_{max}/N_u. The correlation, coherently with a Mohr-Coulomb criterion, is found to be linear, as can be seen in Fig. 9a.

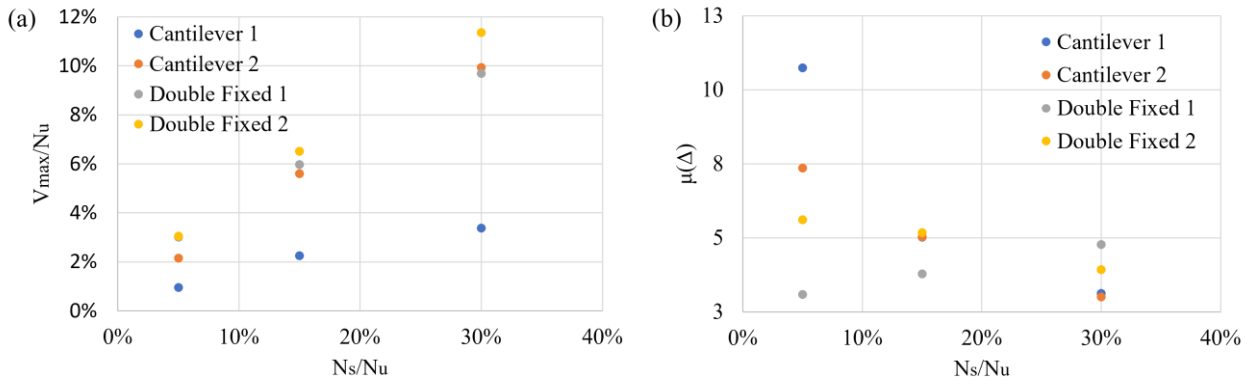

Figure 9 – (a) Maximum dimensionless peak shear and (b) displacement ductility under varying precompression ratio.

When comparing normalized shear loads for all configurations, in fact, value at N_3 level is found to be 3.55, 4.63, 3.22 and 3.73 times higher than that at N_1 level for C1, C2, DF1 and DF2 piers, respectively. Furthermore, as proven by these ratios, this positive correlation seems more relevant for squat (C2 and DF2) piers rather than slender piers.

Similarly, linear relationships were found between N and μ_Δ. However, even though larger displacement capacities were found in association with higher N ratios, the linear relationship between N and μ_Δ is generally found to be decreasing. This is true for both slender (C1) and squat (C2) cantilevered piers- μ_Δ decreasing between 10.75 and 3.12, 7.36 and 3.00, respectively, as well as for squat doubly-fixed piers (DF2), in which ductility decreases between 5.61 and 3.92 with increasing N ratio.

A notable outlier is found in the slender shear-type piers (DF2), in which ductility, ranging between 3.08 and 4.77, increases with applied precompression load. This might be explained by considerations over the interaction between crack pattern and N.

As seen in Section 3.3 (Interpretation of failure modes), applied precompression load plays a key role in the activation of multiple crack bands in squat cantilevered (C2) and slender doubly-fixed (DF1) piers, as well as with phenomena of toe crushing. For DF1 piers the number and magnitude of the relative displacements between blocks by mean of joint sliding is strongly correlated with N ratio. This, coupled with yielding displacements Δ_y - estimated by means of load-displacement curve bilinearization – of the same magnitude for all N ratios, results in an increasing ductility.

Finally, as was foreseeable, higher N_s/N_u ratios are correlated with the development of high normal stress levels in the left corner, hinting at phenomena of toe crushing.

4 CONCLUSIONS

This paper has presented the results of a parametric numerical analysis, which was performed by means of a rigid-block, zero-thickness interface, DE model implemented in 3DEC. The aim of this study was to expand existing knowledge on the behaviour of DSM piers under in-plane loads, which has been limited to experimental tests at interface and wallette scales so far. Structural performance was investigated by means of pushover analysis with displacement control on 12 DSM piers with different boundary conditions, aspect ratios and precompression load.

Numerical results were discussed in terms of load–displacement curves, maximum base shear, displacement ductility, crack pattern, and failure mechanisms. The main conclusions of this study are as follows:

- The rigid-block DE model can successfully simulate the experimental quasi-static in-plane response of DSM wallettes, allowing for the generation of load–displacement relationships and progressive development of crack patterns till structural collapse.
- In line with a Mohr-Coulomb approach, a positive correlation is found between maximum base shear and precompression load, as well as between ultimate displacement and precompression load, which deserves some further considerations.
- The effect of boundary conditions on the in-plane load capacity has been found to be significant, highlighting the higher capacity levels of shear-type, doubly-fixed piers compared to their cantilevered counterparts. By contrast, the higher ductility of cantilevered piers compared to shear-type piers have been quantified, consistently with available experimental data.
- Failure of case-study piers was controlled by sliding shear, so a linear relationship between ultimate load and precompression load has been observed. This has also been confirmed in case of displacement ductility, which however reduces under increasing precompression load as expected.
- The interaction between normal load, boundary conditions and aspect ratios seems to play a key role in failure mechanism and crack pattern, with: a) slender cantilevered piers undergoing rocking failures, b) squat cantilevered and slender doubly-fixed piers being heavily influenced, in terms of crack pattern, by normal load levels, and c) squat doubly-fixed piers undergoing similar mechanisms of sliding shear coupled with toe crushing and disaggregation.

- Overall, a clear relation between the failure mechanism and in-plane capacity of DSM piers has been found.

The positive correlation between ultimate displacement and precompression load, which seems counter-intuitive when considering existing experimental knowledge, might be explained by considering the significant difference, in terms of local behaviour, between mortared and dry-joint masonry. The main local failure mechanism exhibited by DSM, namely joint sliding, is in fact associated with large displacement capacity. Results of this numerical investigation point out that the precompression load influences the distribution of crack pattern, and thus the activation of more phenomena of relative displacement by means of joint sliding. This seems to translate into large displacement capacity in configurations with a diffuse crack pattern. Global phenomena of rocking, instead, contributed to the achievement of large displacement capacity in those cases where crack pattern was more localized. Whenever crack pattern was localized and no rocking occurred, the displacement capacity was smaller.

Further studies, either performed by means of more refined numerical models or through experimental laboratory testing, are needed to shed more light on these findings.

ACKNOWLEDGEMENTS

This study was developed in the framework of the DPC-ReLUIS 2022–2024 project, which is funded by the Italian Department of Civil Protection. The authors would also like to thank Prof. Paulo B. Lourenço and Prof. Daniel V. Oliveira from University of Minho, for kindly sharing their experimental data.

REFERENCES

[1] G. Marzahn, G. König, Experimental investigation of long-term behavior of dry-stacked masonry. *Journal of The Masonry Society*, **12**, 9-21, 2002.

[2] M.J. Greve, C.T. Rapp, J.R. Edwards, C.P.L. Barkan, B. Wilson, Quantification of concrete sleeper and elastic fastening system demands utilizing concrete sleeper rail seat contact area. *Proceedings of the 10th World Congress on Railway Research 2013 (WCRR 2013)*, Sydney, Australia, November 24-27, 2013.

[3] T. Zahra, Z. Yin, M. Dhanasekar, Experimental Investigation of Dry Joint Surface and Closure Characteristics of Interlocking Blocks under Compression. *Proceedings of the 16th International Brick and Block Masonry Conference (IBMaC2016)*, Padova, Italy, June 26-30, 2016.

[4] W.A.M. Thanoon, A.H. Alwathaf, J. Noorzaei, M.S. Jaafar, M.R. Abdulkadir, Finite element analysis of interlocking mortarless hollow block masonry prism, *Computers & Structures*, **86** (6), 520–528, 2008.

[5] P.H.S.W. Kulatilake, S. Shreedharan, T. Sherizadeh, B. Shu, Y. Xing, P. He, Laboratory Estimation of Rock Joint Stiffness and Frictional Parameters, in *Geotechnical and Geological Engineering,* **34** (6), 1723–1735, 2016.

[6] R.L.G. Oliveira, J.P.C. Rodrigues, J.M. Pereira, P.B. Lourenço, H. Ulrich, Normal and tangential behaviour of dry joints in refractory masonry, *Engineering Structures*, **243**, 2021.

[7] P.B. Lourenço, D.V. Oliveira, P. Roca, A. Orduna, Dry Joint Stone Masonry Walls Subjected to In-Plane Combined Loading, *Journal of Structural Engineering*, **131** (11), 1665-1673, 2005.

[8] N.A. Safiee, M.S. Jaafar, A.H. Alwathaf, J. Noorzaei, M.R. Abdulkadir, Structural behavior of mortarless interlocking load bearing hollow block wall panel under out-of-plane loading, *Advances in Structural Eng*ineering, **14** (6), 1185-1196, 2011.

[9] P.B. Lourenco, Computational strategies for masonry structures, PhD Thesis, Delft University of Technology, Delft, Netherlands, 1996.

[10] P.A. Cundall, A computer model for simulating progressive large-scale movements in blocky rock systems, in *Proceedings of the Symposium on Rock Fracture (ISRM)*, vol. 1, paper II-8. Nancy, France, 1971.

[11] P.A. Cundall, Formulation of a three-dimensional distinct element model - Part I: A scheme to detect and represent contacts in a system composed of many polyhedral blocks, *International Journal of Rock Mechanics and Mining Sciences* **25** (3), 107–116, 1988.

[12] J.V. Lemos, Discrete Element Modeling of Masonry Structures, *International Journal of Architectural Heritage*, **1** (2), 190:213, 2007.

[13] B. Pulatsu, S. Gonen, F. Parisi, E. Erdogmus, K. Tuncay, M.F. Funari, P.B. Lourenço, Probabilistic approach to assess URM walls with openings using discrete rigid block analysis (D-RBA), *Journal of Building Engineering*, 61, 2022.

[14] B. Pulatsu, S. Gonen, F. Parisi, Effect of Precompression and Material Uncertainty on the In-Plane Behavior of URM Pier–Spandrel Systems, *Buildings*, **13** (1), 203, 2023.

[15] T.T. Bui, A. Limam, V. Sarhosis, M. Hijaj, Discrete element modelling of the in-plane and out-of-plane behaviour of dry-joint masonry wall constructions, *Engineering Structures*, **136**, 277–294, 2017.

[16] Itasca, 3DEC (2002) – Three Dimensional Distinct Element Code, Version 4.0, Itasca, Minneapolis, 2002.

[17] V. Giamundo, V. Sarhosis, G.P. Lignola, Y. Sheng, G. Manfredi, Evaluation of different computational modelling strategies for the analysis of low strength masonry structures, *Engineering Structures*, **73**, 160-169, 2014.

[18] D.V. Oliveira, Experimental and numerical analysis of blocky masonry structures under cyclic loading, PhD Thesis, Universidade do Minho, Guimaraes, Portugal, 2003.

[19] Z. Liu, A. Crewe, Effects of size and position of openings on in-plane capacity of unreinforced masonry walls, *Bulletin of Earthquake Engineering*, **18**, 4783-4812, 2020.

[20] A.H. Salmanpour, N. Mojsilovic, J. Schwartz, Deformation capacity of unreinforced masonry walls subjected to in-plane loading: a state-of-the-art review, *International Journal of Advanced Structural Engineering*, **5** (22), 2013.

[21] G. Magenes, G.M. Calvi, In-plane response of brick masonry walls, *Earthquake Engineering & Structural Dynamics,* **26**, 1091-1112, 1997.